Longitudinal bunched-beam instabilities going nonlinear: Emittance growth, beam splitting, and turbulence

A. Gerasimov
Fermi National Accelerator Laboratory, P.O. Box 500, Batavia, Illinois 60510
(Received 22 July 1993)

Numerical results of the nonlinear evolution of longitudinal instabilities of bunched beams are presented. Only a pure-dipole instability is considered which appears for the short-bunch, long-wavelength-of-impedance situation, when the wake-field force is a linear function of the coordinate. An argument is made for a rescaling of multibunch dynamics to a single-bunch case for the case of a narrow-band impedance exciting a single coupled-bunch mode. Saturation effects due to the decoherence caused by tune spread are categorized according to the magnitude and type of impedances. The phenomenon of a nonsaturating instability (beam splitting) is described. A slow decay of instabilities after saturation with randomlike bunch-centroid oscillations ("beam turbulence") is observed and discussed.

PACS number(s): 07.77.+p, 41.60.−m, 41.75.−i, 41.85.−p

I. INTRODUCTION

Coherent instabilities of beams in high-energy accelerators due to the interaction with self-induced wake fields were studied extensively over the past decades within the framework of the linearized Vlasov equation. In this approach, one solves for the complex frequency of the small perturbations of the beam density. However, when dealing with an unstable situation, the method applies only to the very early stages of the instability development and is therefore of limited value. Furthermore, the practical issue of emittance growth due to an instability can not be clarified in the linear analysis.

The later nonlinear stages of longitudinal instability evolution for a coasting beam were studied by a few authors [1–3]. Some numerical simulation studies were carried out for the bunched beam, but with the emphasis on a comparison with the linear theory and the thresholds of instabilities [4]. Numerical simulation results [1] indicated that the longitudinal instabilities of a coasting beam always saturate and eventually decay due to the effect of decoherence. A theory of this phenomenon, predicting the energy-spread overshoot was developed in Refs. [2] and [3].

In the present paper, we undertake a numerical simulation study of the late-stage nonlinear development of longitudinal instabilities of bunched beams. Some phenomena observed are quite unusual for the accelerator physics domain and an effort is made to establish a qualitative connection with some esoteric concepts of plasma physics. This may allow a full theoretical description in the future.

The goal of this paper is to study the long-term development of the longitudinal dipole instabilities of bunched beams, with an emphasis on the scenarios of nonlinear saturation and emittance growth. These issues are of considerable importance for the operation of multibunch machines and, in particular, "booster" rings. In the latter, the instabilities can hardly be avoided because of the wide frequency sweeps during the cycle (see, e.g., [5]).

The simulation is carried out for the simplest model which allows for the effects of nonlinear saturation of an instability due to the tune spread in the beam. This model consists of a single bunch interacting with a purely dipole-mode wake-field force (long-wavelength or low-frequency impedance in the classification of Ref. [6]). The long-wavelength condition provides for the domination of the dipole mode in the linear instability analysis [6]. Through the use of that approximation we are able to concentrate on the saturation processes of a purely dipole instability, leaving out all the issues of the mode coupling that become relevant for a shorter wavelength. Notice also that, in spite of a linearized wake force, the problem is fully nonlinear due to the tune dependence on the amplitude. In particular, one can see all higher-order multipole modes developing at the late (nonlinear) stages, out of purely dipole instability.

We present a theoretical argument that our single-bunch model also describes the dynamics of a multibunch system when the impedance is narrow band and peaked near a single revolution harmonic. The results therefore apply to a fairly wide range of realistic situations.

One of the major findings of our study is that the stabilizing effect of the tune spread depends very sensitively on the sign of the coherent frequency shift which is determined by the imaginary part of the effective impedance. When the coherent frequency is shifted from the synchrotron tune in the direction opposite that of the incoherent tune spread (which is always negative for the sinusoidal rf potential), the instability cannot be fully saturated by the decoherence due to the tune spread. One can observe instead that either the whole beam or a part of it that splits off the core oscillates with increasing amplitude without decohering. This beam splitting phenomenon is interpreted as the trapping of particles in the separatrices of self-excited nonlinear resonances, similar to the Bernstein-Greene-Kruskal (BGK) modes in plasma physics.

Simulation results on emittance growth are presented from the perspective of an "overshoot" description. A simple scaling law for emittance growth with the centroid oscillation amplitude is derived for the case of a small synchrotron tune spread.

Late stages of instability development demonstrate a slow decay. The oscillations in this regime become randomlike and the emittance continues growing. This behavior is interpreted as a self-sustained "beam turbulence."

To summarize, the importance of our findings is in the identification of the qualitatively different scenarios for different signs and magnitudes of real and imaginary parts of the effective impedance. Explicit delineation of the parameter regions of the more dangerous regimes, such as beam splitting, can be helpful for choosing better operational conditions of real machines.

The plan of the paper is as follows. In Sec. II we present some theoretical cosiderations regarding the applicability of the model and the scaling of time evolution of observables with the tune spread and impedances. In Sec. III we present the results of numerical simulations. Discussion and conclusions are given in Sec. IV.

II. THEORETICAL CONSIDERATIONS

A. Model

We study the model of the longitudinal dynamics of a bunch interacting with a localized wake field that is represented by the equations

$$\ddot{x}_i + \omega_s^2 x_i - \lambda x_i^3 = \sqrt{\frac{\epsilon}{N}} q \delta_{2\pi}(t) \ ,$$
$$\ddot{q} + \alpha \dot{q} + \omega_c^2 q = \sqrt{\epsilon N} \bar{x} \delta_{2\pi}(t) \ , \tag{1}$$

where time is normalized to make the revolution frequency $\omega_0 = 1$, the quantity x_i is the coordinate of the ith particle of a beam that consists of N particles, $\bar{x}$ is the coordinate of the center of gravity of the beam $\bar{x} = \frac{1}{N}\sum_{i=1}^{N} x_i$, and q is the coordinate of a damped oscillator, coupled to the beam. The oscillator represents the amplitude of an effective single-mode impedance (see below). The interaction is periodic in time and instantaneous ($\delta_{2\pi}$ is a 2π-periodic δ function). The parameter ϵ measures the strength of the interaction in the continuous limit $N \to \infty$ and is related to the conventional notations [6] as $\epsilon = 2\pi e \frac{\omega_0 I_0}{E_0}$ (with e for electron charge, I_0 for the bunch current, and E_0 for the particle energy). Frequencies ω_s and ω_c are, respectively, the synchrotron and resonant impedance frequencies. The constant $\lambda > 0$ measures the nonlinearity of the potential well for the beam particles and is always small in our study. This corresponds to the assumption that the beam occupies a small fraction of the rf bucket(s).

The model (1) can be derived based on the conventional considerations for the longitudinal motion of a single-bunch beam interacting with a single-mode longitudinal wake field, if the bunch length is assumed short relative to the wavelength of the wake field (long-wavelength approximation in the analysis of Ref. [6]) and the impedance is narrow band and nearly resonant. The detailed derivation is presented in Appendix A. The single-mode restriction is manifested in the pure harmonic (single-frequency) oscillations of the wake field q. The condition of the long wavelength of the wake field allows us to keep only the lowest-order dipole-mode interaction (the force that is independent of the coordinate x_i).

It should be emphasized that the linearization of the wake field was not necessitated by the needs of the numerical simulation. Rather, it was used in order to reduce the number of the relevant parameters that define the system and to simplify the physics. It can also be argued that the long-wavelength regime is more important practically as well as theoretically. Indeed, the instability in this case is purely dipole-mode (in the linearized Vlasov analysis) and the issues of the mode coupling that are important for a shorter wavelength (see [6,7]) are not present.

Model (1) also describes the dynamics in the multibunch case under certain conditions. In Appendix B we present the argument for the applicability of model (1) to the multibunch instability with an arbitrary impedance (including the many-modes case), which is peaked near a single revolution harmonic, and for the case of a weak interaction. The bandwidth of the impedance $\Delta\omega_Z$ (the inverse of the characteristic decay time of the wakefield) has to satisfy the condition (i) of restricted bandwidth

$$\delta\omega_s \ll \Delta\omega_Z \ll \omega_0 \ , \tag{2}$$

where $\delta\omega_s$ is the tune spread in the bunches, $\delta\omega_s = \frac{3\lambda}{8\omega_s}\langle x^2 \rangle$, and $\omega_0 = 1$ was left in its dimensional form to emphasize the nature of the approximation. The other condition (ii) is that the interaction must be sufficiently weak:

$$\epsilon \ll \Delta\omega_Z \omega_s^2 \omega_c \ . \tag{3}$$

This condition is often satisfied in cases of practical interest.

B. Stability analysis and scaling laws

Throughout this study we will assume that the condition (i) of restricted bandwidth is satisfied for our model (1) (with $\Delta\omega_Z = \alpha$). The dynamics then can be simplified to a (non-Hamiltonian) collective effective interaction of the particles in the beam as shown in Appendix B:

$$\ddot{x}_i + \omega_s^2 x_i - \lambda x_i^3 = \epsilon \left(-\tilde{Z}_i \bar{x} + \frac{\tilde{Z}_r}{\omega_s} \dot{\bar{x}} \right) \ , \tag{4}$$

where the complex effective impedance $\tilde{Z} = \tilde{Z}_r + i\tilde{Z}_i$ is defined as $\tilde{Z} = Z(\omega_s)$, with the regular frequency-dependent impedance

$$Z(\omega) = -\frac{i}{(2\pi)^2} \sum_n \frac{1}{\omega_c^2 + i\alpha(\omega + n) - (\omega + n)^2} \ . \tag{5}$$

However, for the numerical simulation, we used the original model (1) as it can be cast in the form of discrete-time mapping, which allows a considerable economization of computer time.

The linear stability analysis of model (4) can be done by the conventional linearization of the Vlasov equation (see, e.g., [6]). Since the nonlinearity λ is small, one can use the action-angle variables of the unperturbed linear oscillator, $I = \frac{1}{2\omega_s}\left(\dot{x}^2 + \omega_s^2 x^2\right)$, and $\theta = \tan^{-1}\left(\frac{\dot{x}}{\omega_s x}\right)$ to obtain the dispersion relation for the complex coherent frequency ω of centroid oscillations $\bar{x} = ae^{i\omega t}$:

$$1 = i\epsilon\tilde{Z}\int_c \frac{dI\, I\frac{df_0}{dI}}{\omega^2 - (\omega_s^2 - \lambda' I)}\ , \tag{6}$$

where $\lambda' = \frac{3\lambda}{4\omega_s}$, $f_0(I)$ is the unperturbed normalized density distribution and the integration is along the Landau contour. For a vanishingly small tune spread $\lambda \to 0$ and a weak interaction $|\epsilon\tilde{Z}| \ll \omega_s^2$, the complex coherent frequency shift $\Delta\omega_s = \omega - \omega_s$ is

$$\Delta\omega_s = \frac{i\epsilon\tilde{Z}}{2\omega_s}\ . \tag{7}$$

This defines both the growth rate $\mathrm{Im}(\Delta\omega_s)$ and the (real) coherent frequency shift $\mathrm{Re}(\Delta\omega_s)$.

It is often true under realistic conditions that both the coherent frequency shift $\Delta\omega_s$ and the incoherent tune spread $\delta\omega_s$ are small, so that one can use the approximation (iii) of fast synchrotron oscillations

$$|\Delta\omega_s| \ll \omega_s\ ,\quad |\delta\omega_s| \ll \omega_s\ . \tag{8}$$

This approximation is used in the conventional linear stability analysis (see, e.g., [6]). The synchrotron oscillations then are fast and can be averaged over. For the nonlinear evolution in system (4), the only relevant parameters left are $\delta\omega_s$, $\mathrm{Re}(\Delta\omega_s)$, and $\mathrm{Im}(\Delta\omega_s)$. Any one of these parameters defines the time scale, so that the "slow" evolution of coherent instability depends essentially on two dimensionless parameters

$$C_r = -\frac{\mathrm{Re}(\Delta\omega_s)}{\delta\omega_s}\ ,\quad C_i = -\frac{\mathrm{Im}(\Delta\omega_s)}{\delta\omega_s}\ , \tag{9}$$

where the minus sign was inserted because the nonlinear tune shift is always negative, while the tune spread $\delta\omega_s$ is defined as a positive quantity. The stability border in the C_r, C_i plane for a Gaussian distribution as obtained from our simulation results is shown in Fig. 1.

All quantities pertaining to the coherent instability evolution can be scaled in the form $y = y_0 f_y(\delta\omega_s t, C_r, C_i)$, where y_0 is the initial value and f_y is a dimensionless function of three dimensionless arguments. In the present study we will concentrate on interpreting and categorizing the scenarios of nonlinear evolution in terms of parameters C_r and C_i.

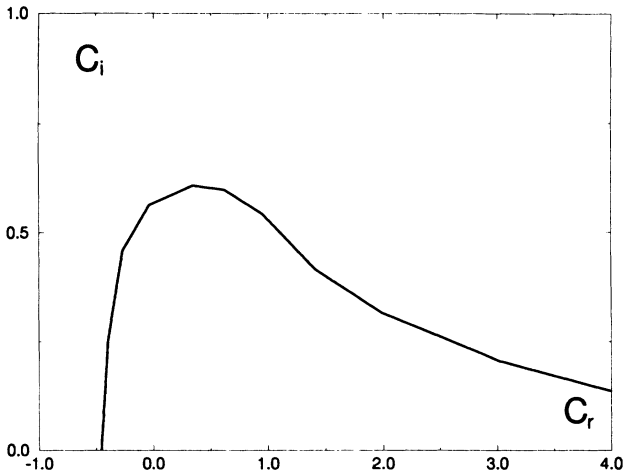

FIG. 1. Stability border for the Gaussian distribution $f_0 \sim e^{-I/(\omega_s\sigma)}$. The area under the curve is stable.

C. Energy balance and emittance growth

The active part of the effective impedance $\tilde{Z}_r$ accounts for the energy loss (when $\tilde{Z}_r < 0$) or production (when $\tilde{Z}_r > 0$) in the system. This is clear for the case of a single particle $N = 1$, when $-\epsilon\frac{\tilde{Z}_r}{\omega_s}$ is the conventional damping decrement. For many particles, the energy balance is obtained from Eq. (4) in the form

$$\frac{dW}{dt} = \frac{\epsilon N\tilde{Z}_r\left(\dot{\bar{x}}\right)^2}{\omega_s}\ , \tag{10}$$

where W is the total energy of the system, comprised of both the incoherent and interparticle interactions:

$$W = \sum_i\left(\frac{\dot{x_i}^2}{2} + \omega_s^2\frac{x_i^2}{2} - \lambda\frac{x_i^4}{4}\right) + \frac{\epsilon N\tilde{Z}_i\left(\bar{x}\right)^2}{2} \tag{11}$$

with $\bar{x} = 1/N\sum_i x_i$.

Under the condition (iii), the parameters ϵ and λ are small, so that the frequency ω_s is a "fast" one. The motion of all particles then is separable into the slow and fast part as $x_i = \sqrt{\frac{2I_i}{\omega_s}}\cos(\omega_s t + \theta_i)$, with both action I_i and angle θ_i being slow variables. Averaging both parts of Eq. (10) over the fast oscillations and dropping the higher-order contributions from nonlinear and interparticle terms in W, one obtains the energy balance equation in the simplified form

$$\frac{dW_0}{dt} = \epsilon N\omega_s\tilde{Z}_r A^2\ . \tag{12}$$

Here the unperturbed energy $W_0 = \sum_i[\dot{x_i}^2/2 + \omega_s^2(x_i^2/2)]$ and centroid oscillations amplitude $A = \sqrt{\dot{\bar{x}}^2/\omega_s^2 + \bar{x}^2}$ [so that $\bar{x} = A\cos(\omega_s t + \varphi)$] are both slow functions of time.

In the slow-fast approximation, it is natural to define the emittance as the average over the fast oscillations $\sigma = 1/N\left\langle\sum_i x_i^2\right\rangle$, so that $\sigma = W_0/N\omega_s^2$. An alternative definition of emittance can be based on the width of the distribution, relative to the center of mass

$\sigma' = 1/N\langle\sum_i (x_i - \bar{x})^2\rangle$. In the slow-fast approximation, these two quantities are related through the amplitude of oscillations A: $\sigma' = \sigma - A^2/2$. Equation (12) defines the rate of emittance growth and can be written as

$$\frac{d\sigma}{dt} = \frac{A^2}{\tau_{\rm gr}} , \tag{13}$$

where $\tau_{\rm gr}$ is the instability rise time in the absence of the tune spread $\tau_{\rm gr} = \frac{1}{{\rm Im}(\Delta\omega_s)}$. This simple scaling of emittance growth is a consequence of the fast synchrotron oscillations approximation (iii) and therefore applies only when the beam fills the small fraction of rf bucket.

III. NUMERICAL SIMULATION

A. Scenarios of evolution: Strong Landau damping

The evolution in model (1) is directly simulated by using many particles and implementing the single-turn mapping. In that mapping, the nonlinearity of oscillations λ is treated perturbatively, i.e., the mapping for

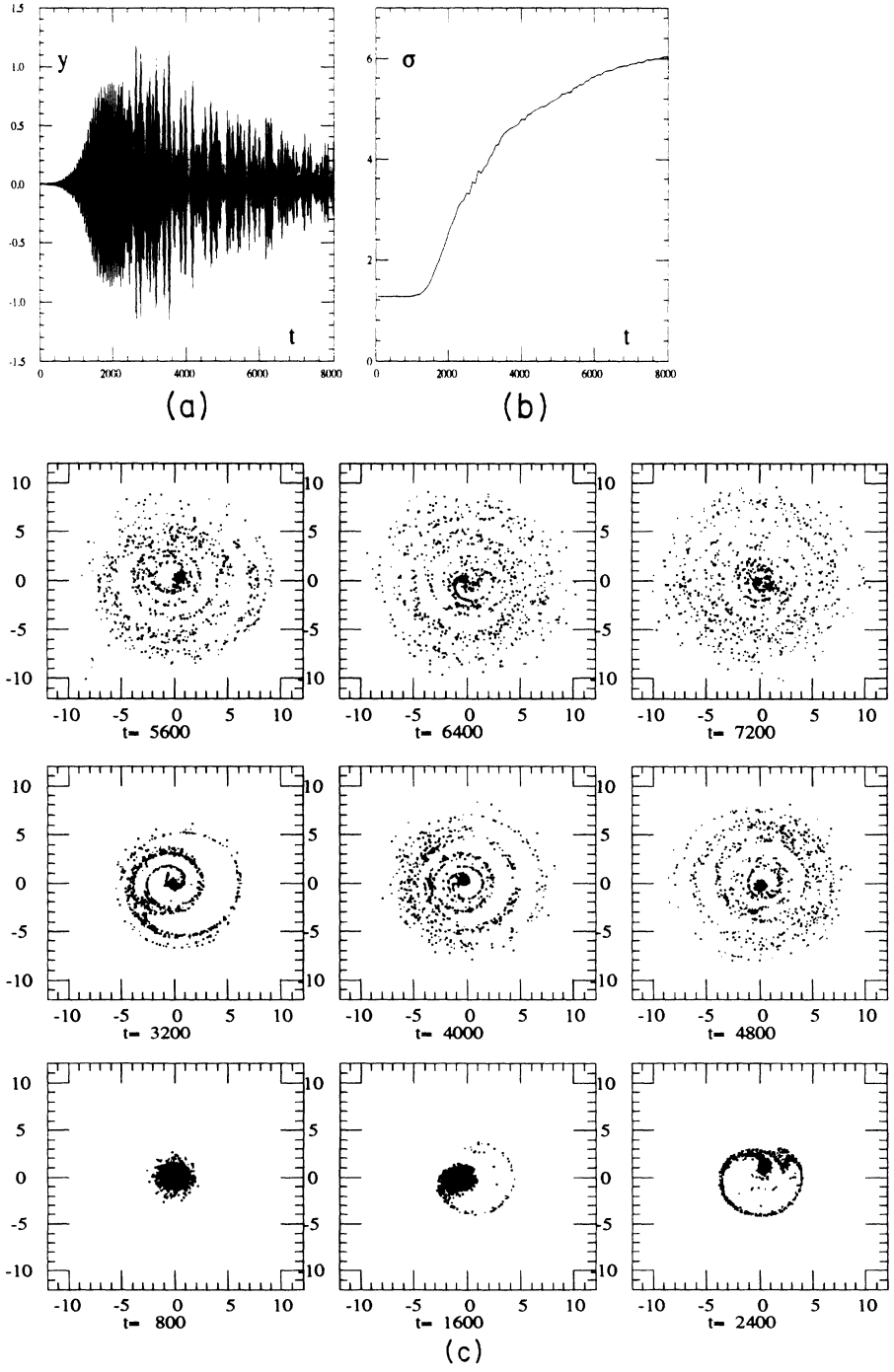

FIG. 2. (a) Centroid oscillations $y = \bar{x}(t)$ and (b) emittance growth $\sigma(t)$ for the case of strong instability, reactive impedance with $C_r = 4.16$, $C_i = 1.65$, and $\tau_{\rm gr} = 188$. (c) Phase-space snapshots for the parameters of (a) and (b).

$x_i, \dot{x}_i$ between the δ-functional "kicks" is that of a linear oscillator with the frequency

$$\omega_s' = \omega_s - \frac{3\lambda}{8\omega_s^2}\left(\frac{\dot{x}_i^2}{2} + \omega_s^2\frac{x_i^2}{2}\right) . \qquad (14)$$

The number of particles N was taken to be large enough to reproduce the continuous limit and in cases close to the instability threshold was as high as $N = 10^5$.

We present the scenarios of instability evolution by dividing all cases in two categories: $C_r > 0$ (strong Landau damping) and $C_r < 0$ (weak Landau damping). The asymmetry of the stability border in C_r as seen in Fig. 1 is indeed quite natural, since when the coherent tune is shifted outside of the nonlinear tune spread, no Landau damping is possible. The asymmetry of the linear stability diagram, however, is much less pronounced for other types of distributions like $f_0 \sim (1 - I/\omega_s\sigma)^2$ (see Ref. [8]) so our terminology is more applicable to the properties of nonlinear saturation than to linear stability.

We first discuss the strong Landau damping $C_r > 0$ category. Four characteristic examples of instability evo-

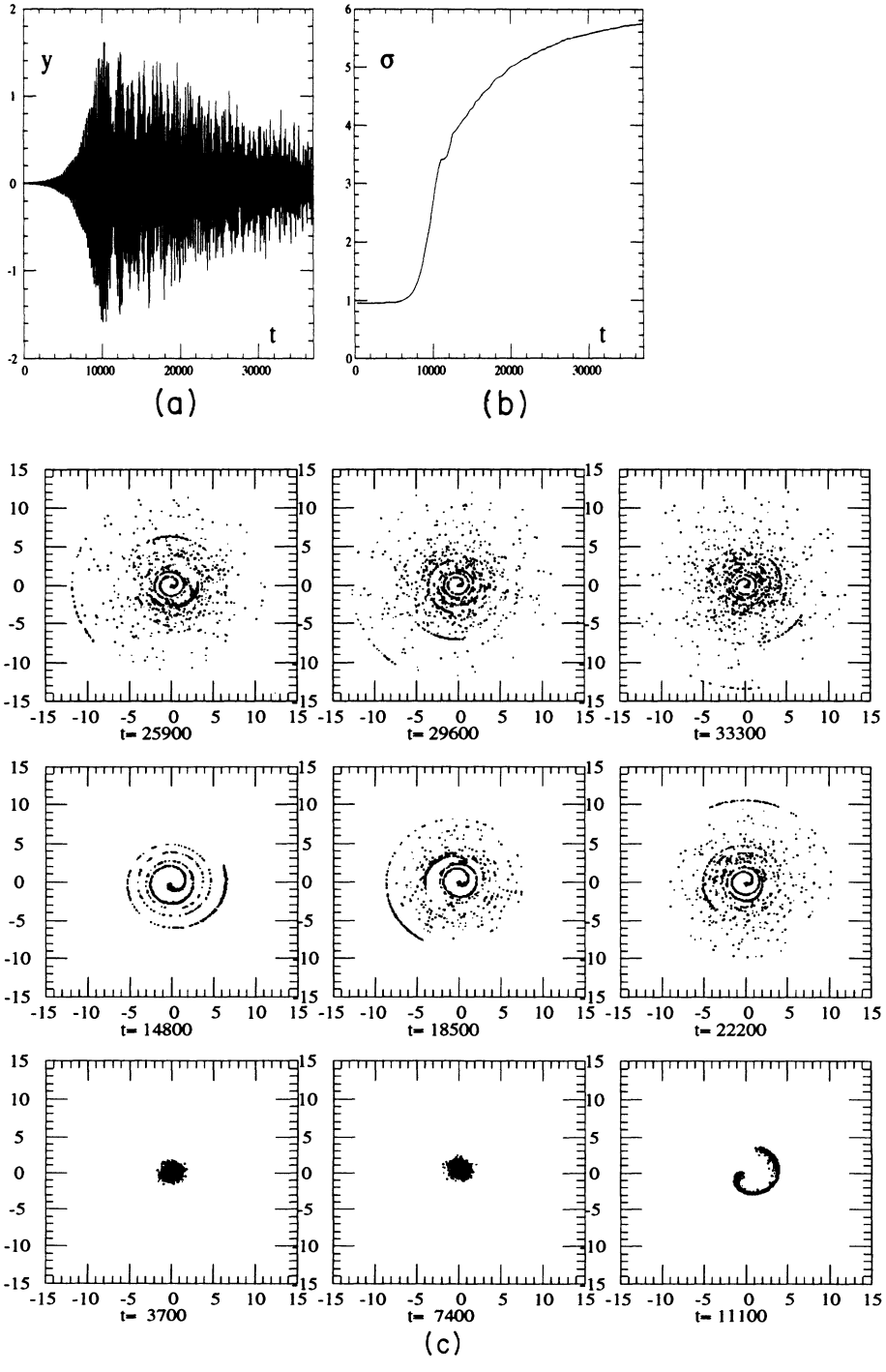

FIG. 3. (a) Centroid oscillations $y = \bar{x}(t)$ and (b) emittance growth $\sigma(t)$ for the case of strong instability, active impedance with $C_r = 1.20$, $C_i = 4.56$, and $\tau_{gr} = 1221$. (c) Phase-space snapshots for the parameters of (a) and (b).

lution in that category are presented in Figs. 2–5. These examples are representative of four different scenarios that we loosely define by the relative strength of the instability (distance from threshold) and the type of impedance: (i) strong instability $C_r \gg C_{r\mathrm{cr}}$, $C_i \gg C_{i\mathrm{cr}}$; (ii) weak instability $C_r \sim C_{r\mathrm{cr}}$, $C_i \sim C_{i\mathrm{cr}}$; (a) reactive impedance $C_r > C_i$ (or $|Z_i| > |Z_r|$); and (b) active impedance $C_r < C_i$ (or $|Z_i| < |Z_r|$).

The quantities $C_{r\mathrm{cr}} = C_{r\mathrm{cr}}(C_r/C_i)$ and $C_{i\mathrm{cr}} = C_{i\mathrm{cr}}(C_r/C_i)$ are the critical (i.e., corresponding to the stability border) values for a given value of the ratio C_r/C_i. The quantity C_i is positive in all examples (negative C_i corresponds to the stable beam).

An example of scenario (i),(a) (strong instability, reactive impedance) with parameters $C_r = 4.16$ and $C_i = 1.65$ is shown in Fig. 2. The time dependence of the centroid oscillations $\bar{x}(t)$ is plotted in Fig. 2(a). Emittance growth as a function of time $\sigma(t)$ is shown in Fig. 2(b). Samples of the corresponding phase space snapshots are shown in Fig. 2(c). Time is measured in number of

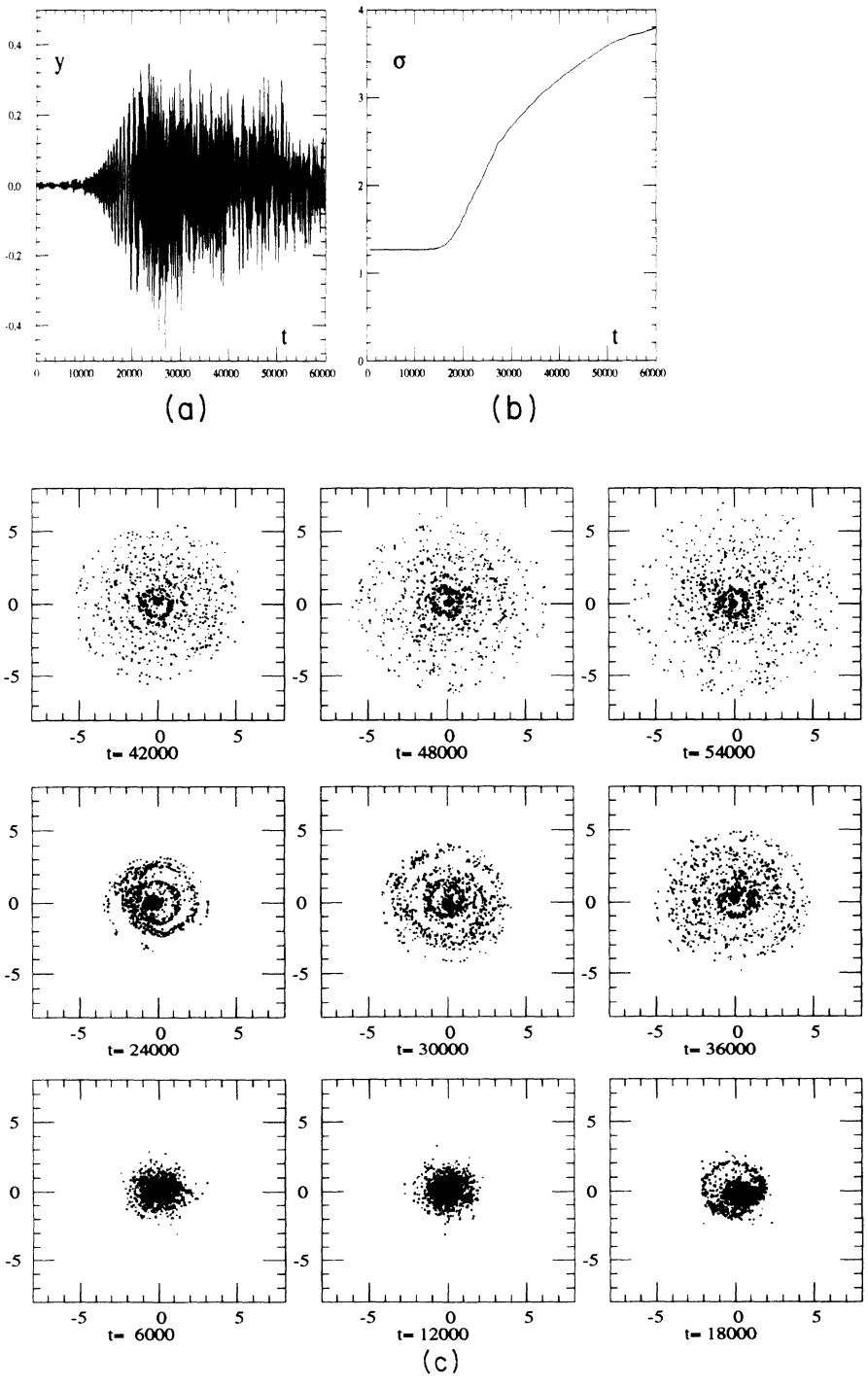

FIG. 4. (a) Centroid oscillations $y = \bar{x}(t)$ and (b) emittance growth $\sigma(t)$ for the case of weak instability, reactive impedance with $C_r = 1.25$, $C_i = 0.49$, and $\tau_{\mathrm{gr}} = 315$. (c) Phase-space snapshots for the parameters of (a) and (b).

turns [number of "kicks" in model (1)]. The instability rise time in the absence of tune spread is $\tau_{gr} = 188$ turns.

The centroid oscillations in Fig. 2(a), as well as in all other cases to follow, presents itself as a fast-oscillating sinusoidal signal (with the synchrotron frequency) with a slowly changing envelope, since the parameters are chosen so as to satisfy condition (iii). The slow evolution in Fig. 2(a) demonstrates three consecutive stages: (1) initial monotonic growth, (2) saturation at some rather high level (comparable to the size of the beam), and (3) slowly decaying oscillations of apparently random nature ("turbulence"). Transition from smooth "laminar" envelope to the "turbulent" behaviour occurs approximately at the saturation point. The monotonic growth of the envelope of oscillations until saturation is the characteristic feature of a strong instability regime.

Emittance evolution is shown in Fig. 2(b). The maximum rate of emittance growth is occuring roughly at the saturation point. After saturation the emittance growth slows down considerably. We interpret it as a turbulent regime with slowly decaying quasirandom oscillations.

In Fig. 2(c) the phase-space snapshots of the distribu-

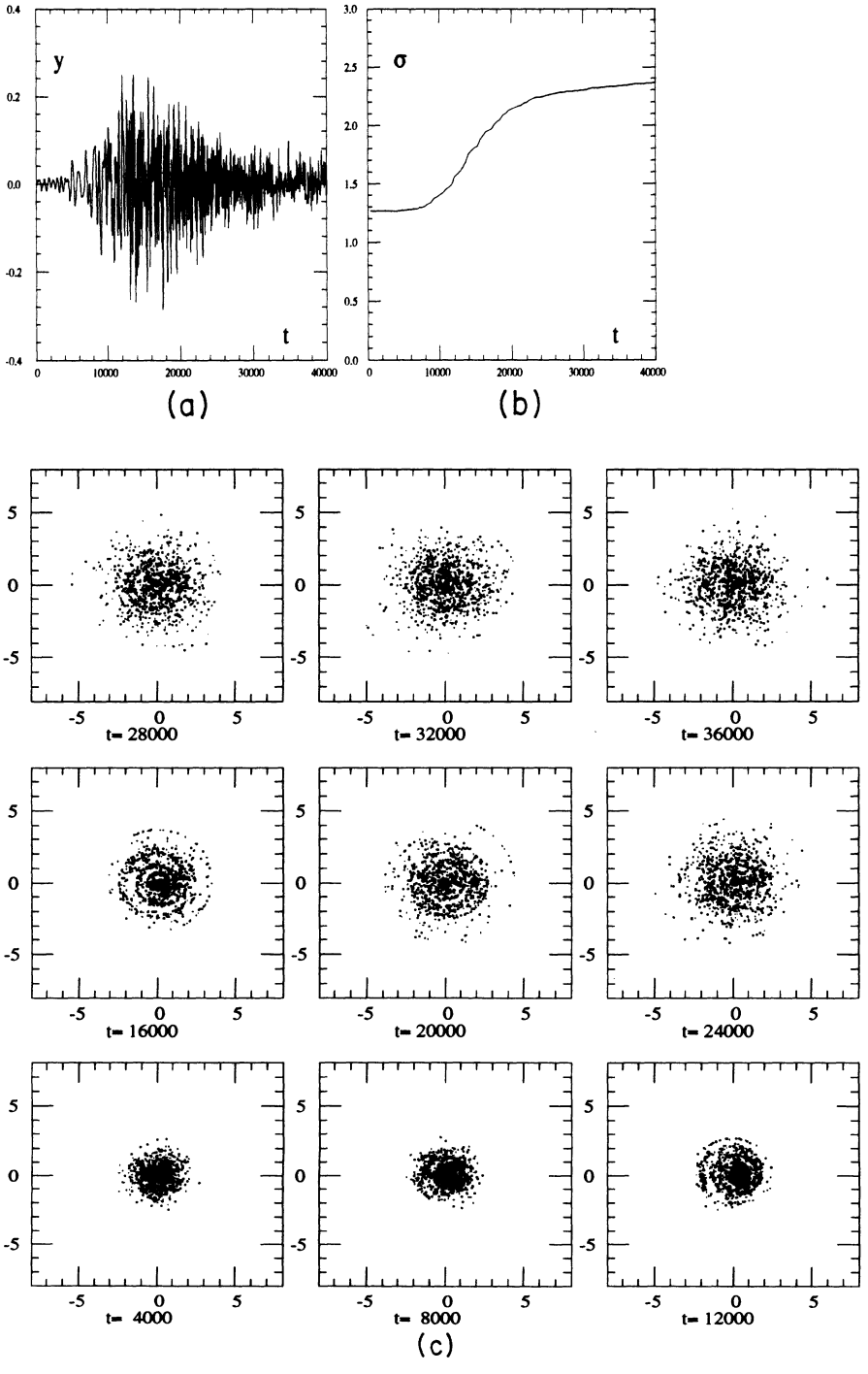

FIG. 5. (a) Centroid oscillations $y = \bar{x}(t)$ and (b) emittance growth $\sigma(t)$ for the case of weak instability, active impedance with $C_r = 0.24$, $C_i = 0.89$, and $\tau_{gr} = 175$. (c) Phase-space snapshots for the parameters of (a) and (b).

tion are shown for ten equidistant moments of time over the time span of evolution in Figs. 2(a) and 2(b). These snapshots provide some insight into the nature of the processes leading to saturation and turbulence. One interesting property is that until saturation the bunch oscillates with increasing amplitude as a single entity without any visible effect of decoherence due to the tune spread. Closer to saturation, the bunch develops a thin "tail" of particles trailing behind it. After that, the bunch is losing particles to its tail, diminishing in size, and returning back to the center of origin. The spiral-like tail of particle density that the central bunch left behind is gradually decohering due to the phase mixing. The remnants of the higher-density bunch near the center continues to maintain some small-scale motion, as the thin tail of that bunch is discernible for a long time.

An example of scenario (i),(b) (strong instability, active impedance) for $C_r = 1.20$ and $C_i = 4.56$ is shown in Fig. 3. The time dependence of centroid oscillations is presented in Fig. 3(a). The time scale is determined by $\tau_{\rm gr} = 1221$ turns. The general pattern of evolution is similar to the previous case. The initial stage up to saturation is the monotonic growth of the oscillations. After saturation, the oscillations become randomlike and decay slowly.

Emittance growth as a function of time is shown in Fig. 3(b). After saturation, the emittance growth is slowing down. A series of phase-space snapshots is shown in Fig. 3(c). One feature of this series that is different from the previous case is that the particles that are located at larger radia (amplitude of oscillations) at the moment of saturation start moving toward increasing amplitudes in a sicklelike formation. This structure persists for some time, though particles are apparently being lost in the course of the radial motion, producing a sparce "tail" of density at large radia. We view this structure as a weak remnant of "trapped modes" that are observed for the weak Landau damping regime $C_r < 0$, which is discussed in Sec. III B.

An example of scenario (ii),(a) (weak instability, reactive impedance) for $C_r = 1.25$ and $C_i = 0.49$ is shown in Fig. 4. This case corresponds to about the same ratio C_r/C_i as for the case of Fig. 2 and can represent then the same impedances but lower interaction strength ϵ (current in the ring).

The time dependence of the centroid motion is presented in Fig. 4(a). The time scale is defined by $\tau_{\rm gr} = 315$. An important distinction from the previous cases is that the envelope of oscillations is not a monotonically growing function of time even before the saturation. The signature of the weak instability, as observed from this and other graphs, is threefold: (1) the initial growth rate of the instability is very slow, as one would expect from the linear theory; (2) the first maximum in the envelope of the oscillations occurs early before the saturation and is quite small, and it is followed by several more maxima of increasing amplitude before the saturation; and (3) maximally attainable amplitudes of centroid oscillations are much smaller than in the case of a strong instability.

Emittance growth as a function of time is shown in Fig. 4(b). The saturation point on the emittance curve is less pronounced than in the case of a strong instability.

In Fig. 4(c) the phase-space snapshots of the distribution are shown for ten equidistant moments of time over the time span of evolution in Figs. 4(a) and 4(b). Most of the structure (radial and angular inhomogeneities) can be seen at $t = 18\,000$ and $t = 24\,000$, which are the moments of time close to when the saturation occurs.

An example of scenario (ii),(b) (weak instability, active impedance) for $C_r = 0.24$ and $C_i = 0.89$ is shown in Fig. 5.

The time dependence of the centroid motion is presented in Fig. 5(a). The time scale is defined by $\tau_{\rm gr} = 175$ turns. All properties of the weak instability (1)–(3) are true in this case as well. An apparent randomization of oscillations is happening before saturation. The decay of these after the saturation is quite slow and does not appear to be determined by any relevant time constant of the system. Remember here that what looks like broadband oscillations in Fig. 5(a) is still a relatively slowly modulated sinusoidal signal, since the time scale plotted is quite long.

Emittance growth as a function of time is shown in Fig. 5(b). Small undulations on the curve are real (not a computational artifact) and correspond to the local maxima in the envelope of oscillations of Fig. 5(a). As in previous examples, the emittance growth after saturation is slowing down but does not disappear altogether.

In Fig. 5(c) the phase-space snapshots of the distribution are shown for ten equidistant moments of time over the time span of evolution in Figs. 5(a) and 5(b). Little structure can be discerned and one can only notice that azimuthal and radial inhomogeneities of the density are quite irregular even before the saturation (which happens at about $t = 14\,000$).

B. Scenarios of evolution: Weak Landau damping

In the case of weak Landau damping $C_r < 0$ the scenarios of evolution are qualitatively different from the strong Landau damping case $C_r > 0$. Two examples for different ratios C_r/C_i are presented in Figs. 6 and 7.

An example of evolution of a relatively strong instability (not close to the threshold) with the active type of impedance (with parameters $C_r = -0.64$ and $C_i = 2.96$) is shown in Fig. 6. Centroid oscillations and emittance as functions of time are shown in Figs. 6(a) and 6(b). The striking feature of these plots is that the instability does not saturate, as the centroid oscillations grow to the level of seven times the initial size of the beam and continue growing. More insight into this behavior is provided by the phase snapshot series of Fig. 6(c).

Until the moment of time $t \sim 12\,000$ the bunch oscillates as a whole, while after that it decoheres into a spiral-like structure. After $t \sim 16\,000$, the outmost particles form a sicklelike "beamlet" that splits off the rest of the distribution and oscillates as a rigid entity with increasing amplitude. It is this nondecohering beamlet that causes unlimited growth of centroid oscillations and emittance in Figs. 6(a) and 6(b).

An example of instability with even weaker Landau

damping (larger negative C_r, reactive impedance) with parameters $C_r = -2.89$ and $C_i = 1.61$ is shown in Fig. 7. Centroid oscillations and emittance time dependences in Figs. 7(a) and 7(b) again indicate an unlimited growth. The phase space snapshot series in Fig. 7(c) shows that here nearly all particles are going into the nondecohering sicklelike formation and just a tiny part of the bunch is left near the center.

We suggest the term "beam splitting" for the phenomenon of a nonsaturating instability through the formation of nondecohering "beamlets" (or whole beams). The border of the beam splitting region in the plane C_r, C_i was verified by many additional runs to be defined by the line $C_r = 0$ and the stability border of Fig. 1. It was observed also that the border is a "soft" one, i.e., the percentage of particles trapped in the beamlets approaches zero when approaching the border. In some cases one can also see several beamlets successively splitting from the core of the distribution.

It can be important to suggest the possible devel-

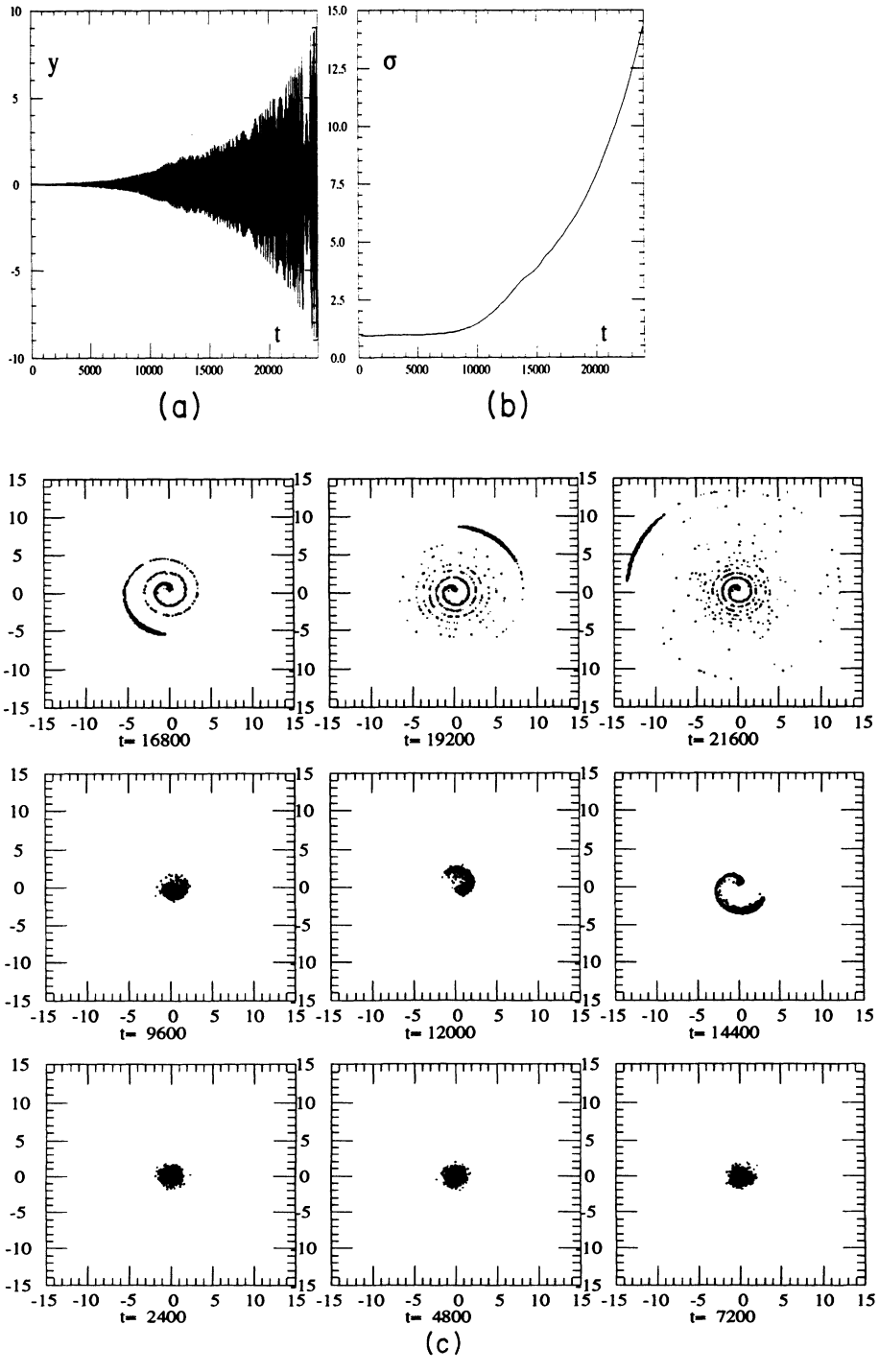

FIG. 6. (a) Centroid oscillations $y = \bar{x}(t)$ and (b) emittance growth $\sigma(t)$ for the case of weak instability, active impedance with $C_r = -0.64$, $C_i = 2.96$, and $\tau_{gr} = 1880$. (c) Phase-space snapshots for the parameters of (a) and (b).

opment, in the realistic environment, of the oscillation growth that is unlimited in our model. This can be done upon the realization that there are two approximations that will cease to be valid when the amplitude of oscillations grows too large: the condition of the fast synchrotron oscillations (8) and the condition of the long wavelength of impedance. Accordingly, there are two mechanisms that can stop the growth of oscillations: first, when the oscillating beamlet approaches the separatrix of the rf bucket and, second, when the amplitude of oscillations becomes comparable to the impedance wavelength. The first mechanism will dominate when the rf wavelength is longer than the impedance wavelength. The oscillations will stop to grow, however, at much higher amplitude than in the strong Landau damping regime.

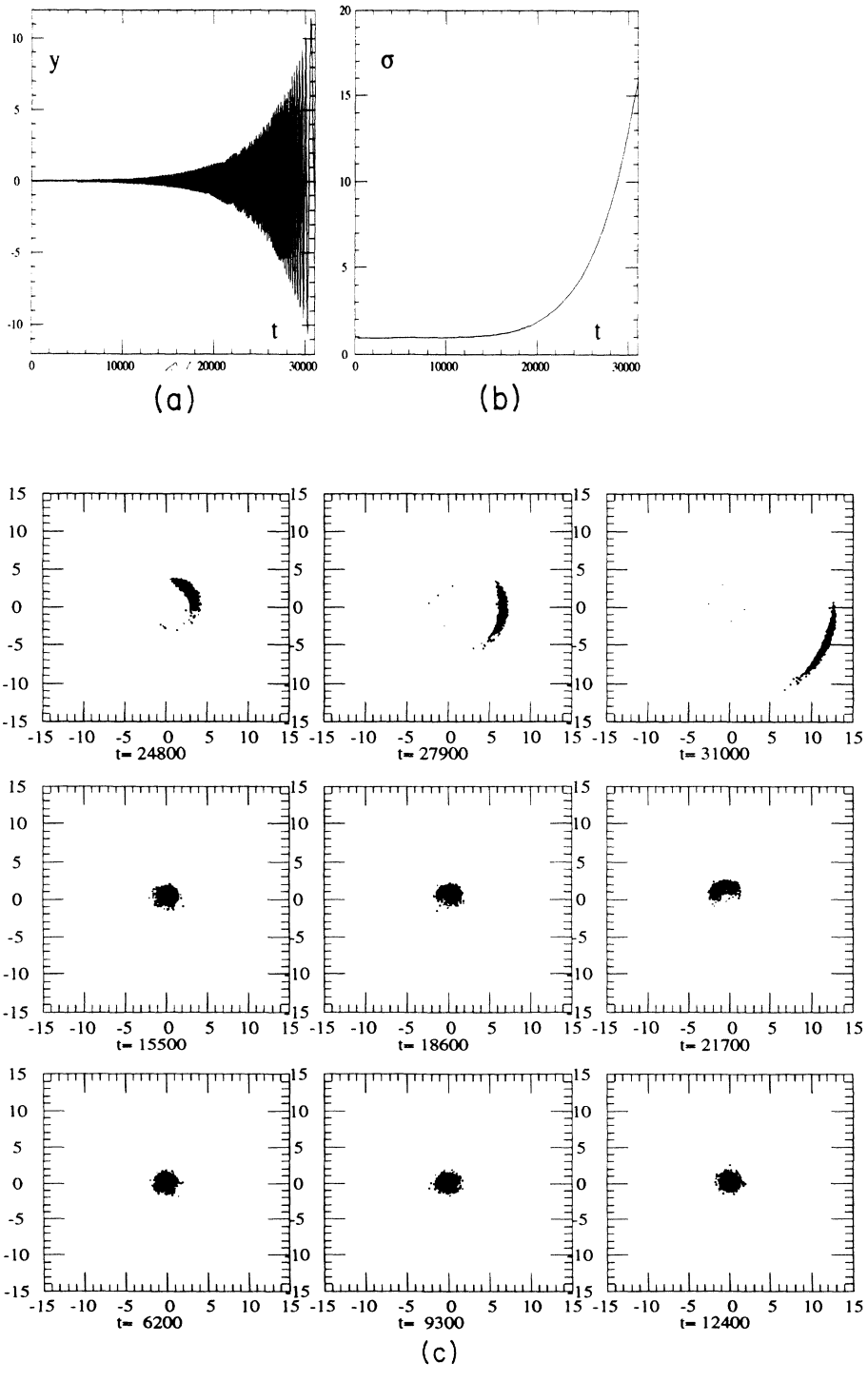

FIG. 7. (a) Centroid oscillations $y = \bar{x}(t)$ and (b) emittance growth $\sigma(t)$ for the case of weak instability, active impedance with $C_r = -2.89$, $C_i = 1.61$, and $\tau_{gr} = 3455$. (c) Phase-space snapshots for the parameters of (a) and (b).

C. Emittance growth and overshoot

In the past, substantial effort was dedicated to study, both in theory and in simulation [1–3], the energy spread blowup due to longitudinal instabilities of coasting beams. The main result of these studies was the identification and analysis of the overshoot phenomenon. This implies that the instability is always transient and gradually dies away when the spread is increasing above the critical value. The term overshoot specifically alludes to the dependence of the final spread on the initial: the smaller is the latter, the larger the former.

In the bunched-beam model in the weak Landau damping regime $C_r < 0$ the instability does not saturate and the concept of the overshoot does not apply. For strong Landau damping $C_r > 0$, however, the approach is justified and we studied the emittance growth process from that perspective. The results of these simulations, when the initial emittances were changed while keeping the impedances $\tilde{Z}_r, \tilde{Z}_i$ constant, are presented in Figs. 8 and 9.

In Fig. 8, the case of active impedance with the ratio $C_i/C_r = 5.38$ is shown. The basic pattern of emittance growth in this case follows the overshoot scenario. Slight deviations from this scenario though are noticable as well, as one can see some pairs of curves intersecting twice. Another feature is the sharp rise of emittance growth for $\sigma(0) < 1$. It is associated somehow with the transient sicklelike structures as seen in Fig. 3(c).

In Fig. 9, the rise of emittance growth with the lowering of $\sigma(0)$ is more gradual than in Fig. 8. One can again see some peculiarities in emittance growth near the instability threshold, with the curves intersecting twice. It can also be noticed that near the threshold the emittance does not always completely saturate, but rather continues some slow growth. We return to the discussion of this phenomenon in the next subsection.

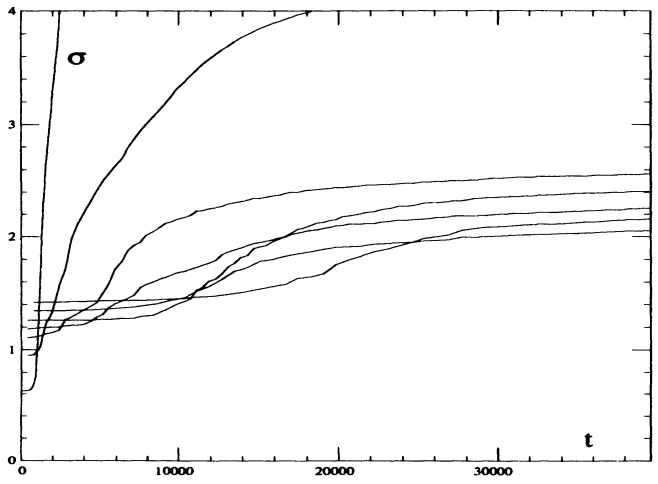

FIG. 8. Emittance growth $\sigma(t)$ for different inital values $\sigma(0)$. The impedances ratio is $C_i/C_r = 5.38$.

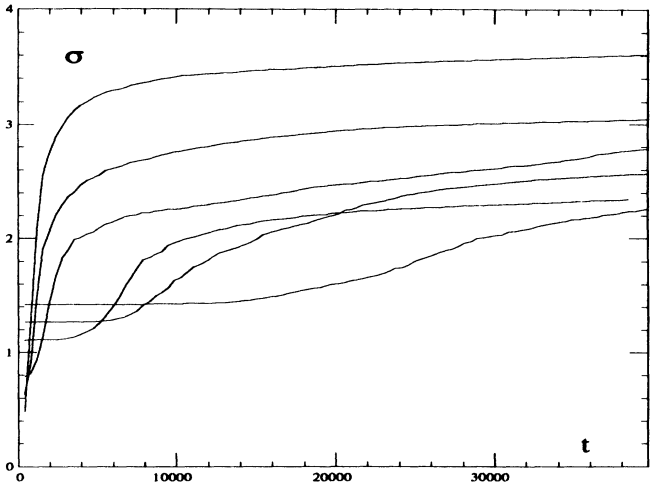

FIG. 9. Emittance growth $\sigma(t)$ for different inital values $\sigma(0)$. The impedances ratio is $C_i/C_r = 1$.

D. Beam turbulence

Centroid oscillations after the saturation in the strong Landau damping regime $C_r > 0$ appeared to a certain degree random in all the examples that were given so far. To quantify this randomness, we took a series of power spectra of relatively short sections of centroid oscillations $\bar{x}(t)$. The length of the series was chosen to cover the duration of the period up to and around the saturation. The centroid oscillations and emittance growth for this example are shown in Figs. 10(a) and 10(b). The values of $C_r = 1.12$ and $C_i = 1.12$ are not very close to the stability border (see Fig. 1). In Fig. 10(a), one can see the distinct irregular outbursts of centroid oscillations after saturation that also produce small irregular steps in the curve $\sigma(t)$ in Fig. 10(b) in accordance with the emittance growth scaling law (13).

In Fig. 10(c) we present the series of the power spectrum evolution for the sections of the signal $y(t)$ of Fig. 10(a). The whole period was divided in ten sections, and time labels refer to the end of each section. Different plots were scaled vertically to have the same height of the peaks. Before the saturation at about $t = 3000$ the spectra are clearly single peaked and quite narrow. After the saturation (the plot at $t = 3816$), the spectrum becomes broader several times and develops a multipeaked structure. This proves our thesis of the randomization of oscillations, or the onset of turbulence, after the saturation.

The question of the long-term behavior of the instability was touched upon in Sec. III C. It appeared from the data in that section that the instability, at least in some cases, does not completely decay after the saturation. Instead, one observes low-level quasirandom (turbulent) centroid oscillations that persist for a long time after the saturation and cause a slow emittance growth. One more example of a long-term evolution of this kind for the case of Figs. 10(a) and 10(b) is given in Fig. 10(d). The

sensitivity of the long-term turbulent emittance growth to the number of particles in the simulation is very high ($N = 3 \times 10^5$ particles were required to reproduce the continuous limit in this case).

The phase-space plots after the saturation in all previous examples show only small azimuthal inhomogeneities that are hardly discernable by eye. That is the case as well for the turbulent stage of Fig. 10. To provide more insight into the nature of the turbulence, we present in Fig. 10(e) a few line density profiles for the case of Figs. 10(a) and 10(b). One can see that the turbulent regime corresponds to the presence of a short-wavelength low-amplitude "microstructure" or "jitter" on top of a smooth density profile. This microstructure undergoes relatively fast [on the scale of the time span of Figs. 10(a)–10(e)] variations that appear to be random.

IV. DISCUSSION AND CONCLUSIONS

The physics of the observed nonlinear phenomena of saturation, beam splitting, and turbulence is far from being fully clarified by our numerical findings. This calls for a future study, and we would like to make a few suggestions in that direction.

The most striking of all nonlinear effects observed is the nonsaturating instability, beam splitting phenomenon that happens for the weak Landau damping regime $C_r < 0$. We suggest that this may be interpreted as the trapped-particle nonlinear modes, in extension of a similar concept of persistent nonlinear (BGK) waves in plasma physics (see, e.g., [9]). We expect by that analogy that in our system a group of particles can stay, under certain conditions, near the center of the self-driven non-

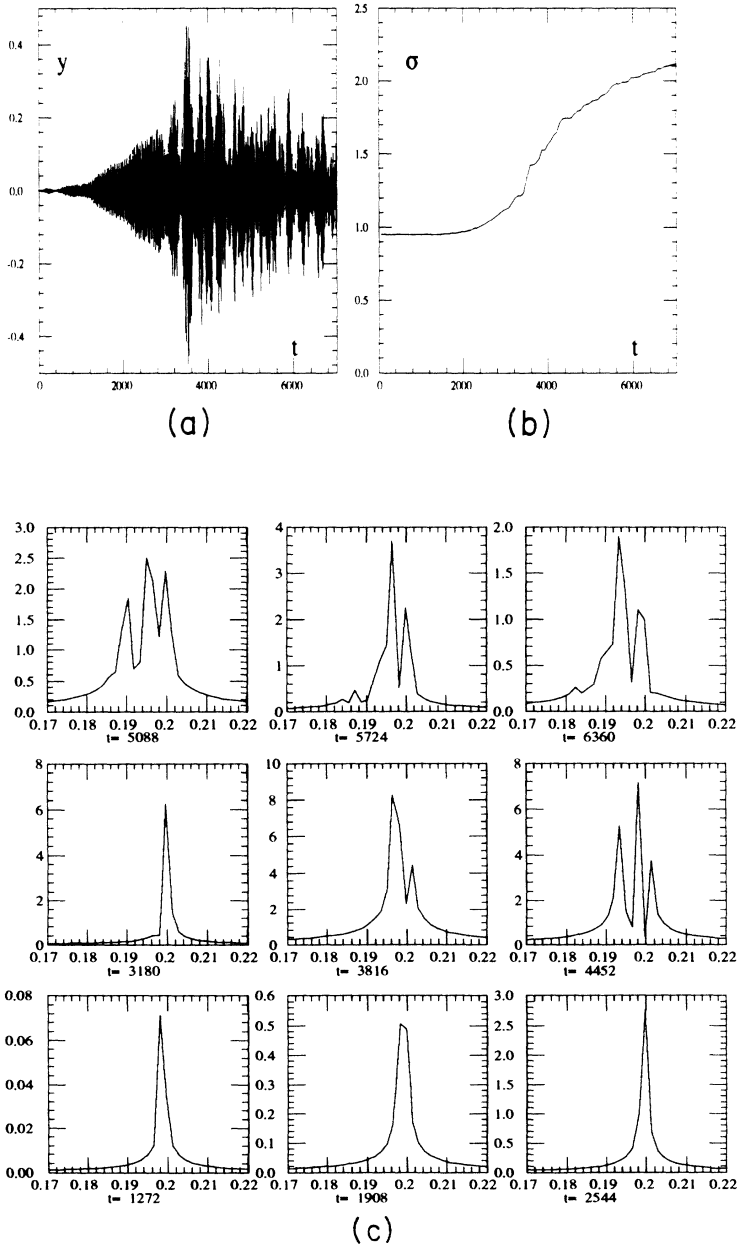

FIG. 10. Beam turbulence: oscillation randomization after saturation. (a) Centroid oscillations $y = \bar{x}(t)$ and (b) emittance growth $\sigma(t)$ for the case $C_r = 1.12$, $C_i = 1.12$, and $\tau_{gr} = 122$. (c) Evolution of short-term power spectrum of centroid oscillations in (a). The synchrotron frequency is $\omega_s = 0.2$. (d) Nondecaying low-level turbulence for the case of (a) and (b). (left) Centroid oscillations $y = \bar{x}(t)$ and (right) emittance growth $\sigma(t)$ for the case $C_r = 1.12$, $C_i = 1.12$ and $\tau_{gr} = 122$. (e) Line density profiles evolution for the case of (a) and (b).

linear resonance. The elongated shape of the beamlets in Figs. 6(c) and 7(c) corraborates that interpretation, since that is what one would expect to see for a distribution of particles near the center of a narrow resonance.

The conceptual importance of the BGK modes in plasma physics stems from the fact that they present themselves as persistently oscillating states where no energy exchange between the particles and the wave is taking place. In our case, the energy is pumped into the system by the real part of the impedance [see Eq. (10)] and persistent steady-state oscillations are impossible. The trapped (BGK) modes for our system can be visualized as the states without any Landau damping, with the amplitude of a dipole oscillation increasing in time by taking the energy from the external source (which is eventually the rf system). The resonant frequency will change as well, while the particles stay inside the separatrix of the resonance as it moves towards larger radia. The difference with conventional BGK modes is in this (anti)dissipation in the system that causes the frequency sliding. Thus we suggest the term "sliding trapped (BGK) modes." A preliminary result is that these modes exist only for the weak Landau damping regime $C_r < 0$, conforming with our observations of instability development scenarios. One can anticipate obtaining a theoretical description of beam splitting phenomenon on the basis of this approach.

Beam turbulence is another class of essentially nonlinear phenomena. Even after saturation when the emittance becomes large enough to make a beam stable for

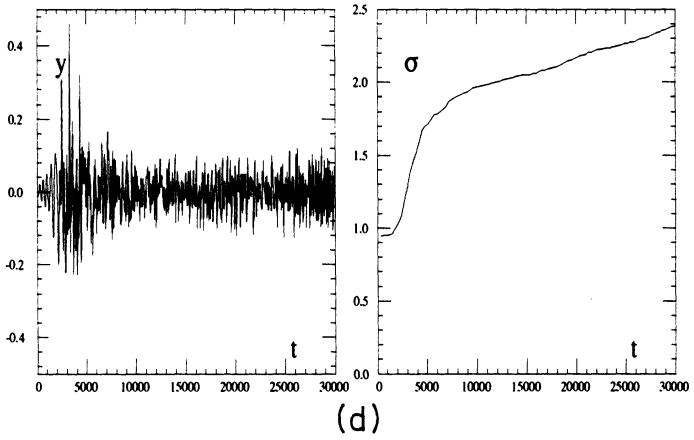

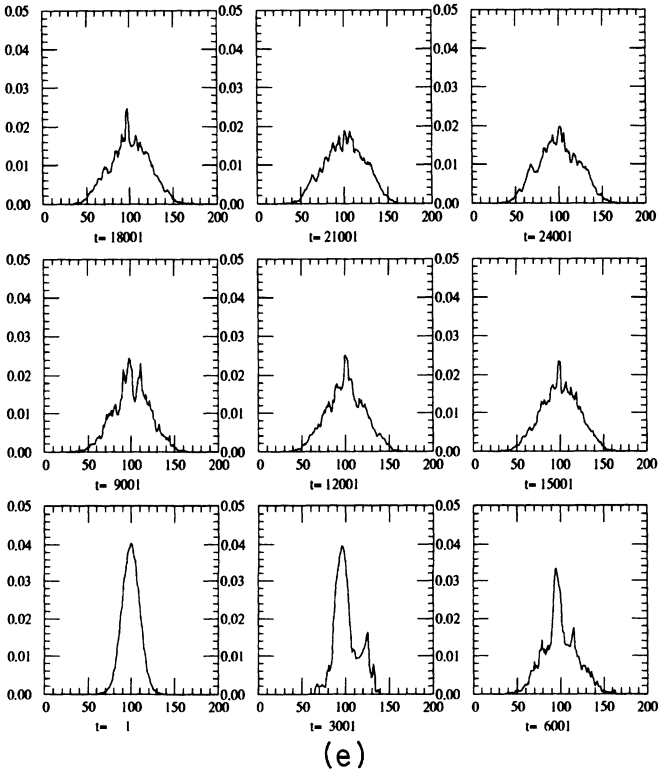

FIG. 10 *(Continued).*

any smooth bell-shaped distribution, the small-scale "microstructure" of the density can persist in the beam for a long time, causing low-level centroid oscillations and slow emittance growth. This may be an issue of practical importance and requires a further study.

Emittance growth is related to the amplitude of the centroid oscillations through the convinient scaling law (13). The self-consistent theoretical prediction of how the oscillations will evolve is, however, very difficult. Some estimates of this kind were obtained in a quasilinear overshoot approach [10] along the same lines as in the coasting beam theory [2,3]. However, these are based on the single-mode approximation and may not work well for the weakly unstable case when the turbulence sets in early before saturation.

ACKNOWLEDGMENTS

I would like to acknowledge many useful discussions with Pat Colestock. His advice and encouragement were essential. The Fermi National Accelerator Laboratory is operated by the Universities Research Association, Inc. under contract with the U.S. Department of Energy.

APPENDIX A

In this appendix, we show how to derive the linearized-wake-field model (1) from a generic wake-field (single-bunch) model under the condition of the Long wavelength of the impedance. The general expression for the collective force in the time domain is (see, e.g., [7])

$$F(x,t) = \kappa \sum_{l=0}^{\infty} \int dx' \rho(x', t - lT_0) W(lL_0 + x' - x) \ , \tag{A1}$$

where $\rho(x,t)$ is the line density of the beam, $W(x)$ is the wake-field function, T_0 is the revolution period, L_0 is the circumference of the ring, and the summation is over all preceding revolutions. The intensity parameter κ is $\kappa = e\frac{\omega_0 I_0}{E_0}$ (with e for electron charge, I_0 for the bunch current, and E_0 for the particle energy) [6]. The form (A1) is equivalent to a more familiar frequency-domain representation when the line density perturbation ρ' is a harmonic function of time:

$$F'(x,t) = -i\kappa \sum_p \rho'_p Z(p+\Omega) e^{i(px - \Omega t)} \ , \tag{A2}$$

where ρ'_p are the Fourier harmonics $\rho'(x,t) = \sum_p \rho'_p e^{i(px-\Omega t)}$ and $Z(\omega)$ is the impedance $Z(\omega) = \int dx e^{i\omega x \frac{T_0}{L_0}} W(x)$. The condition of the long wavelength of the wake field relative to the bunch length can be used in expanding all the terms $l \neq 0$ in the wake field W (A1) up to linear terms in the small argument $x' - x$. In the $l = 0$ term, one can use the same condition by substituting for the wake field $W(x)$ by the step function of x. This yields the force as the sum $F = F_0 + F'$ of an incoherent (ρ-independent) part F_0 and a coherent part F':

$$F_0(x) = \kappa \sum_{l=1}^{\infty} W(lL_0) - \kappa x \sum_{l=1}^{\infty} W'(lL_0) \ ,$$
$$F' = \kappa \int_x^{\infty} dx' \, \rho(x',t) + \kappa \sum_{l=0}^{\infty} \bar{x}(t - lT_0) W'(lL_0) \ , \tag{A3}$$

where $\bar{x}(t) = \int dx' x' \rho(x',t)$ is the centroid coordinate and $W' = \frac{dW}{dx}$ is the wake-field derivative. The incoherent time-independent component F_0 produces a shift in the equilibrium synchrotron phase (which accounts for the parasitic energy loss) and a change of the synchrotron frequency. Both of these quantities are small under the assumption of weak interaction (3) and (8) and will be neglected in what follows.

The first term in the coherent component F' corresponds to the single-pass contribution to the potential well distortion in the absence of coherent oscillations. In general, it produces a contribution to the tune spread $\delta\omega' \sim \kappa$. In the case of a narrow-band nearly resonant impedance, however, this extra tune spread is much smaller than the unperturbed tune spread $\delta\omega_s$. By the same token, in the presence of coherent oscillations, the dipole mode contribution of the first term in F' is much smaller than the second term for the case of a narrow-band nearly resonant impedance. In other words, the multiturn wakes in this case are much larger then the single-turn ones. We are left finally with the dominant term in the wake force in the form

$$F = \kappa \sum_{l=0}^{\infty} \bar{x}(t - lT_0) W'(lL_0) \ . \tag{A4}$$

In our model (1), where the wake field is localized (the interaction is δ functional) the collective force $F = \sqrt{\epsilon/N} q \delta_{2\pi}$ can be expressed as

$$F(t) = \epsilon \delta_{2\pi} \sum_{n=0}^{\infty} \bar{x}\left([t]_{2\pi} - 2\pi n\right) G(t - [t]_{2\pi} - 2\pi n) \ , \tag{A5}$$

where $[t]_{2\pi}$ is the moment of time of the last "kick" $[t]_{2\pi} = 2\pi[t/2\pi]$ ([ ] denotes the integer part). The quantity G is given by

$$G(t) = \sin(\omega_r t) e^{\omega_i t} \ , \tag{A6}$$

where $\omega_r + i\omega_i = -i\alpha/2 + \sqrt{-\alpha^2/4 + \omega_c^2}$. This expression becomes equivalent to the distributed wake (A4) if one utilizes the condition of the synchrotron frequency being much smaller than the revolution frequency $\omega_s \ll 1$. Indeed, averaging $F(t)$ (A5) over the "fast" time scale $\Delta t = 2\pi$ yields

$$\bar{F}(t) = \frac{\epsilon}{2\pi} \sum_{n=0}^{\infty} \bar{x}([t]_{2\pi} - 2\pi n) G(2\pi n) \ . \tag{A7}$$

This is equivalent to the expression (A4) [with a specific

choice of $W'(x) = G(2\pi x/L_0)$ (A6) and $\kappa = \epsilon/2\pi$] since $\bar{x}(t)$ changes very little over the revolution period $\Delta t = 2\pi$.

APPENDIX B

Consider a multibunch longitidinal motion with a localized impedance of a long wavelength:

$$\ddot{x}_i^{(n)} + \omega_s^2 x_i^{(n)} - \lambda \left(x_i^{(n)}\right)^3 = \sqrt{\frac{\epsilon}{N}} q \delta_{2\pi}\left(t + 2\pi \frac{n}{M}\right) , \tag{B1}$$

$$\ddot{q}_l + \alpha_l \dot{q}_l + \omega_{cl}^2 q_l = \sqrt{N} \sum_{n=1}^{M} \sqrt{\epsilon_l} \bar{x}^{(n)} \delta_{2\pi}\left(t + 2\pi \frac{n}{M}\right) ,$$

where $q = \sum_l q_l \sqrt{\epsilon_l/\epsilon}$ is the sum over different modes q_l with different frequencies ω_{cl} and damping decrements α_l which are coupled to the beam with a different coupling strength ϵ_l. Furthermore, M is the number of bunches and $x_i^{(n)}$ is the coordinate of the ith particle in the nth bunch. The representation of the wake field in (B1) is fairly general as one can represent an arbitrary spectrum of impedance as a superposition of Lorentzian curves.

We assume now that the dominant modes of the wake field are tuned near only one of the coupled-bunch mode frequencies $|\omega_c - (\mu + kM)| \ll 1$ (here μ is the coupled-bunch integer index between 1 and M) and that the width of the impedance peak near that coupled-bunch frequency is small $\Delta\omega_z \ll 1$ [right-hand side of condition (i)]. These conditions allow us to have a single coupled-bunch mode dominating the dynamics.

As a next step, we assume that the interaction is weak $\epsilon \ll \alpha_l \omega_s^2 \omega_{cl}$ [condition (ii)] and the tune spread is small $\lambda\langle x^2\rangle \ll \omega_s^2$. The first condition is necessary for the introduction of an effective impedance. The centroid oscillations $\bar{x}^{(n)}(t)$ then can be separated into the fast synchrotron oscillations with the frequency ω_s and a slowly changing envelope:

$$\bar{x}^{(n)} = a \cos\left(\omega_s t + 2\pi \frac{n\mu}{M} + \varphi\right) , \tag{B2}$$

where the amplitude a and the phase φ are slow functions of time. Expanding the periodic δ function in Fourier series, one finds the dominant response of the cavity at positive and negative synchrotron sidebands of the resonant coupled-bunch frequency:

$$q = \frac{\sqrt{N}}{2\pi} \sum_l \sqrt{\frac{\epsilon_l}{\epsilon}} \mathrm{Re}\left[\frac{a\, e^{i[(\omega_s+\mu+kM)t+\varphi]}}{\omega_{cl}^2 - (\omega_s+\mu+kM)^2 + i\alpha_l(\omega_s+\mu+kM)} + \frac{a\, e^{i[(\omega_s-\mu-kM)t+\varphi]}}{\omega_{cl}^2 - (\omega_s-\mu-kM)^2 + i\alpha_l(\omega_s-\mu-kM)}\right] . \tag{B3}$$

In Eq. (B1), the two-time scale approximation allows us to retain only the Fourier component of the collective force $F = \sqrt{\epsilon/N} q \delta_{2\pi}(t + 2\pi \frac{n}{M})$ at the frequency ω_s, yielding

$$\ddot{x}_i^{(n)} + \omega_s^2 x_i^{(n)} - \lambda \left(x_i^{(n)}\right)^3 = \epsilon \mathrm{Re}\left[i\tilde{Z} a e^{i(\omega_s t + \varphi + 2\pi \frac{n}{M})}\right] , \tag{B4}$$

where $\tilde{Z}$ is the effective impedance $\tilde{Z} = Z(\omega_s)$. The impedance $Z(\omega)$ is

$$Z(\omega) = -\sum_l \frac{i\sqrt{\epsilon_l/\epsilon}}{(2\pi)^2}\left[\frac{1}{\omega_{cl}^2 - (\omega+\mu+kM)^2 + i\alpha_l(\omega+\mu+kM)} + \frac{1}{\omega_{cl}^2 - (\omega-\mu-kM)^2 + i\alpha_l(\omega-\mu-kM)}\right] . \tag{B5}$$

One can now extract the equation for the slowly varying quantities a and φ directly from Eq. (B4). Using the alternative slow variables for the centroid $\bar{y} = a\cos\varphi$, $\dot{\bar{y}} = -a\omega_s \sin\varphi$ and for individual particles $y_i = a_i \cos\varphi_i$, $\dot{y}_i = -a_i\omega_s \sin\varphi_i$, one obtains after averaging over the fast oscillations

$$\ddot{y}_i + \omega_s^2 y_i - \frac{3}{8}\lambda(y_i^2 + \dot{y}^2/\omega_s^2)^{3/2} = \epsilon\left(-\tilde{Z}_i \bar{y} + \frac{\tilde{Z}_r}{\omega_s}\dot{\bar{y}}\right) . \tag{B6}$$

Equivalently, one can return to the initial variables $x_i = x_i^{(0)}, \dot{x}_i = \dot{x}_i^{(0)}$ and present the averaged equations of motion in the form

$$\ddot{x}_i + \omega_s^2 x_i - \lambda x_i^3 = \epsilon\left(-\tilde{Z}_i \bar{x} + \frac{\tilde{Z}_r}{\omega_s}\dot{\bar{x}}\right) . \tag{B7}$$

In our single-bunch, single-mode wake-field model (1), the effective impedance $\tilde{Z}$ is defined by only one term in the sum in expression (B5). Since one can achive arbitrary values of $\tilde{Z}_r$ and $\tilde{Z}_i$ by adjusting ω_c and α, the single-bunch model is fully equivalent, under specified restrictions, to the multibunch system (B1).

[1] E. Keil and E. Meserschmid, Nucl. Instrum. Methods **128**, 203 (1975).
[2] Y. Chin and K. Yokoya, Phys. Rev. D **28**, 2141 (1983).
[3] S. Bogacz and K.-Y. Ng, Phys. Rev. D **36**, 1538 (1987).
[4] R. H. Siemann, Nucl. Instrum. Methods **221**, 293 (1984).
[5] K. Harkay, P. Colestock, and A. Gerasimov, in *Proceedings of the 1993 IEEE Particle Accelerator Conference, Washington, DC* (IEEE, New York, in press).
[6] C. Pelligrini, in *Physics of High Energy Particle Accelerators,* edited by R. Carrigan, F. Huson, and M. Month, AIP Conf. Proc. No. 87 (AIP, New York, 1982), p. 77.
[7] A. Chao, in *Physics of High Energy Particle Accelerators (Stanford Linear Accelerator Center, Stanford University, California)*, Proceedings of lectures presented at the Second Annual U.S. Summer School on High Energy Particle Accelerators, edited by Melvin Month, AIP Conf. Proc. No. 105 (AIP, New York, 1982).
[8] F. Sacherer, CERN Report No. CERN/MPS/BR, 73-1, 1973 (unpublished).
[9] T. Stix, *The Theory of Plasma Waves* (McGraw-Hill, New York, 1993).
[10] A. Gerasimov (unpublished).